Journal of
Marine Science and Engineering

MDPI

Article

Seafloor Sediment Acoustic Properties on the Continental Slope in the Northwestern South China Sea

Guanbao Li [1,2,*], Jingqiang Wang [1,2], Xiangmei Meng [1,2], Qingfeng Hua [1,2], Guangming Kan [1,2] and Chenguang Liu [1,2]

1 Key Laboratory of Marine Geology and Metallogency, First Institute of Oceanography, MNR, Qingdao 266061, China; wangjqfio@fio.org.cn (J.W.); mxmeng@fio.org.cn (X.M.); hqf@fio.org.cn (Q.H.); kgming135@fio.org.cn (G.K.); lcg@fio.org.cn (C.L.)
2 Laboratory for Marine Geology, Qingdao Marine Science and Technology Center, Qingdao 266237, China
* Correspondence: gbli@fio.org.cn

Abstract: The acoustic properties of seafloor sediments on continental slopes play a crucial role in underwater acoustic propagation, communication, and detection. To investigate the acoustic characteristics and spatial distribution patterns of sediments on the continental slope, a geoacoustic experiment was conducted in the northwestern South China Sea. The experiment covered two sections: one crossing the shelf and slope in the downslope direction, and the other near the shelf break in the along-slope direction. In situ techniques, sediment sampling, and laboratory measurements were used to acquire data on sediment acoustic properties (such as sound speed and attenuation) and physical properties (including particle composition, density, porosity, and mean grain size). The experimental findings revealed several key points: (1) Acoustic properties of shallow water coarse-grained sediments and deep-sea sediments were higher when measured in the laboratory compared to in situ measurements. (2) Relationships between measured attenuation and physical properties, as well as between sound speed and mean grain size, showed deviations from previous empirical equations. (3) Sediment acoustic and physical properties exhibited significant variations in the downslope direction, while showing gradual variations in the along-slope direction. These variations can be attributed to sedimentary environmental factors such as material sources, hydrodynamic conditions, and water depth.

Keywords: sound speed; attenuation; sediment; continental slope; continental shelf; in situ measurement; South China Sea

check for updates

Citation: Li, G.; Wang, J.; Meng, X.; Hua, Q.; Kan, G.; Liu, C. Seafloor Sediment Acoustic Properties on the Continental Slope in the Northwestern South China Sea. *J. Mar. Sci. Eng.* **2024**, *12*, 545. https://doi.org/10.3390/jmse12040545

Academic Editor: Dimitris Sakellariou

Received: 28 February 2024
Revised: 20 March 2024
Accepted: 21 March 2024
Published: 25 March 2024

1. Introduction

The acoustic properties of sediments, including sound speed, attenuation, and density, play a crucial role in the transmission and reflection of sound waves in seafloor sediments and at the sediment–water interface [1]. Understanding these properties is essential for underwater navigation, communication, and detection using acoustic techniques [2]. These properties are influenced by sediment composition, texture, and depositional processes, making them valuable in marine sedimentary environments, marine engineering, and oceanographic studies [3,4]. Acoustic properties of sediments vary spatially, depending on sediment distribution patterns shaped by environmental conditions during formation [5,6]. Hamilton's 1980 study in the North Pacific Ocean categorized sediment acoustic and physical properties into three physiographic provinces: continental terrace, abyssal plain, and abyssal hill [6]. Among these provinces, continental terrace, including continental shelf and slope, exhibit diverse sediment types and complex acoustic property variations, thus large impacts on the sound propagation.

Over the past two decades, studies have focused on the frequency-dependence of sediment acoustic properties, especially for sandy sediments [7–12], with data collection primarily in shallow or coastal areas. A few investigations and studies were carried out on sediment acoustic property distribution in continental slope regions. Wang et al. [13] investigated acoustic properties of surface sediments in the South China Sea, finding higher sound speeds on shelves compared to slopes and troughs. Kim et al. [4] studied the sound speed distribution of surficial sediments in the Ulleung Basin, east of the Korean Peninsula, and identified geoacoustic provinces reflecting sediment textures and properties consistent with marine geological features in shelf and slope environments. Tian et al. [14] analyzed sound speed data from sediment samples at 270 stations in the northern South China Sea, identifying two geoacoustic provinces consistent with water depth, and they found that sound speed ratios were less than 1 in the relatively deeper slope region and more than 1 in shallower shelf region, and the latter was further divided into two sub-provinces based on sediment type. Studies mentioned above are all based on sediment acoustic data obtained by sampling and laboratory measurement methods, although some have attempted to make in situ corrections using seafloor temperatures and water pressures [4]. However, comparison between in situ and laboratory measurements in the west Pacific Ocean deeper than 5000 m had showed the limitations in fully correcting laboratory sound speed into the in situ one in the deep waters due to structural perturbations and state changes of sediment sample [15]. This hinders accurate recognition of spatial variability of acoustic properties based solely on laboratory measurement data. Furthermore, most previous studies, including that of Hamilton [6], lacked analysis of spatial distribution of acoustic attenuation.

In recent years, in situ sediment acoustic measurement techniques were rapidly developed in China and widely used in the field survey (e.g., [15–17]), providing a technical basis to overall and accurately understand the distribution of sediment acoustic properties, not only sound speed, but also attenuation. Using a hydraulic-driven in situ sediment acoustic measurement system, Li et al. [18] observed strong down-slope variations and relative along-slope uniformity of sound speed and attenuation in the northern South China Sea, implying the peculiarity of sound property distribution on the continental slope. However, due to the sparsity of measurement stations and lacking sediment samples, detailed analysis of the sedimentary environment was not provided. To further understand sediment acoustic property variations on the continental slope and their environmental controlling factors, a sediment acoustic experiment based on in situ and laboratory acoustic measurement techniques was conducted on the northwestern South China Sea (SCS), along two sections, one parallel and the other perpendicular to the slope. The results of this experiment and some new findings are presented in the following.

2. Regional Settings

The experimental area is situated in the northwestern SCS (Figure 1), extending southeastward from the middle part of continental shelf near Hainan Island to the Xisha Trough, with water depth ranging from 90 m to 1900 m. The Xisha Trough is a northeast-trending depression located on the western continental slope of the South China Sea, serving as a transition zone between the northwest shelf and the central basin of the South China Sea.

Different current systems dominate the shelf and the slope. The SCS northwestern shelf is influenced by the Guangdong Coastal Current (GCC), which shifts direction seasonally due to monsoon climate, flowing northeastward in summer and southwestward in winter [19]. The Xisha Trough is affected by the SCS Deep Water Current (DWC), which originates from the Pacific Ocean, enters SCS through the Luzon strait, and flows southwest along the SCS northern slope into Xisha Trough [20].

Sediments in this region come from nearby large rivers (e.g., the Pearl River, and Red River) and small mountain rivers (e.g., the rivers on Hainan and Taiwan Island) [21–23]. These sediment sources, along with the flow patterns, determine the distribution of sediment types in the area. Various sediment types are found in the shelf area [23,24], arranged roughly in a northeast-trending belt. Offshore of Hainan Island, there are gravelly sands which transition to silty sands, sandy silt, and clayey silt as one moves away from the island. Fine sands are also locally present, along with a layer of muddy sediments on the inner shelf near Hainan Island. From the outer part of the shelf to the Xisha Trough, clayey silt is the dominant sediment type [24].

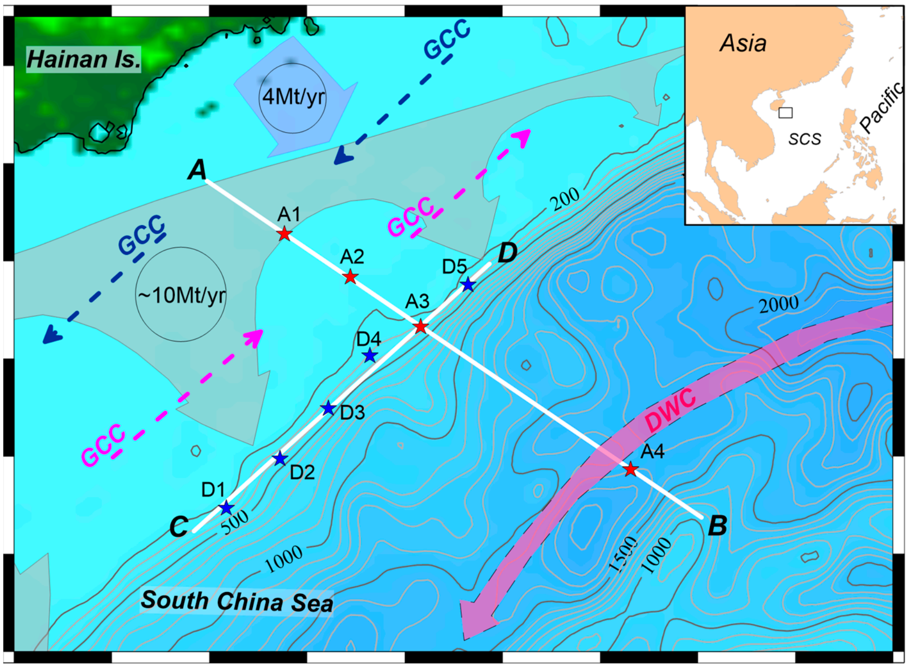

Figure 1. Location map of the two sections (solid while lines) and stations (pentagrams in red and blue, respectively) in the experiment. The upper right inlet shows the location of the study area. The dashed line with an arrow indicates the flow direction of the GCC (dark blue for winter, pink for summer), modified from Liu et al. [25]. The thick solid-brown line with arrows indicates the direction of the DWC (modified from Zheng and Yan [20]). Grey arrows depict sediment transport paths from the Red River, while light-blue arrows show transport from the Wanquan River on Hainan Island, with the arrow size indicating discharge amount (according to Zhao et al. [26]). Isobaths at 100 m intervals are represented by light-grey solid lines, with bathymetry data sourced from GEBCO [27].

3. Materials and Methods

The goal of the experiment is to study the distribution and variation pattern of sediment acoustic properties on the continental slope and its adjacent shelf, so two near-perpendicular sections in cross-slope and along-slope directions, respectively, were established as depicted in Figure 1. Section AB, approximately perpendicular to the isobath direction, comprises four stations: A1 and A2 in the shelf area (depth ~100 m), A3 out of the shelf break (depth 244.4 m), and A4 in the Xisha Trough center (depth 1864.8 m). In situ measurements were conducted at all these stations using the ballast in situ acoustic measurement system (BISAMS), with sediment samples collected simultaneously using a short gravity corer attached on BISAMS for acoustic and physical property measurement in laboratory. Section CD, roughly parallel to the isobath direction, includes stations D1–D5 and intersects section AB at station A3. These six stations are all near the shelf break, with water depths mostly between 350 m and 400 m, except for D4 (depth ~300 m). In situ measurements were not performed at D1–D5 due to the bad weather conditions, and only sediment samples were collected using a gravity corer.

The BISAMS used for in situ measurements on section AB has been previously described (e.g., [15,17]). This system is capable of measuring in situ sound speed and attenuation at a depth of 80 cm below the seafloor, using a 30 kHz central frequency and a 10 MHz sampling frequency. The BISAMS consists of four acoustic transducers, one transmitter and three receivers, which penetrate the seafloor under the pressure of the ballast weight. The transducers transmit and receive pulse waveform signals which passes through the sediment. The sound speed and attenuation can be calculated using the travel time difference and amplitude difference of the signals received by three channels (Figure 2), respectively, according to the formula suggested by Wang et al. [17]. During each measurement at a station, the waveform signals were transmitted and received six times, and the averaging algorithm was used to eliminate the noise. Furthermore, the average value of three receiving channels is used to reduce measurement error. The BISAMS demonstrates stable performance and high measurement accuracy, and has been utilized in seafloor acoustic measurement expeditions in the East China Sea [17], the South China Sea [28], and the west Pacific Ocean [15].

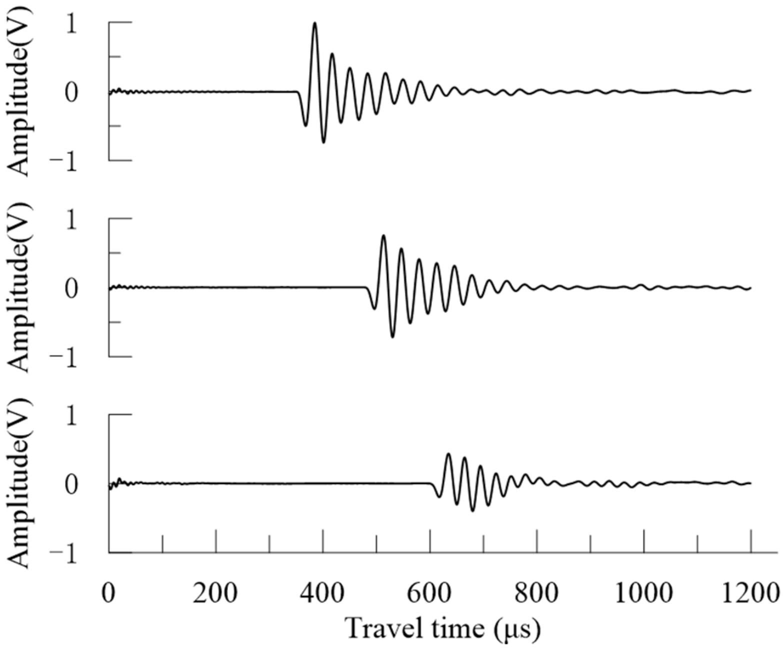

Figure 2. Pulse waveform signals acquired using three receiving channels of BISAMS.

The ratio of sediment sound speed to the seawater sound speed under the same temperature and pressure conditions is defined as the sound speed ratio (SSR), which is experimentally and theoretically proved to remain constant [29–31]. During the experiment, a self-contained sound speed profiler (SVP, Valeport Ltd., Devon, UK) was attached to the BISAMS, and the seawater sound speed was acquired simultaneous at each in situ measurement. Then, the SSR is calculated as the ratio of sediment sound speed measured using the BISAMS to near-seafloor seawater sound speed measured using the SVP.

The BISAMS is equipped with a 75 mm diameter short gravity corer, so a sediment sample with length equivalent to the penetration depth can be collected synchronously during the situ measurement of section AB. For sections CD, the sediment sampling was conducted only, using a 110 mm diameter, 3 m long gravity corer. All sediment samples were measured in laboratory for acoustic and physical property.

In the laboratory, sound speed and acoustic attenuation were measured with an acoustic measurement system, as detailed by Wang et al. [32], which comprises a digital signal generator and a waveform recorder, a power amplifier and a preamplifier, a couple of transmitting and receiving planar transducer with central frequency of 100 kHz, and an acoustic measuring platform. The sample was segmented into 20–30 cm lengths and placed on the platform. Acoustic signals at 100 kHz frequency were emitted and received by transducers at the sample ends. Sound speed was determined using the time-of-flight (TOF) method based on signal travel time and sample length. Acoustic attenuation coefficients were calculated by comparing signal amplitudes and propagation path lengths between full-length and segmented samples using the coaxial gap attenuation measurement method [15,33]. For each segment sample, the sound speed and attenuation were measured at least three times, and the laboratory sound speed and attenuation values were obtained by averaging segment measurements. Sample temperature was recorded, and the sound speed in seawater at that temperature (with salinity of 35‰) was calculated using Mackenzie's formula [15]. The ratio of laboratory sediment sound speed to seawater sound speed was defined as the laboratory sound speed ratio. Sound attenuation coefficient measurements, whether in situ or in the laboratory, were divided by frequency to determine the attenuation factor [3,6].

Following the acoustic measurement, the samples underwent physical property measurements to determine parameters such as particle composition, mean grain size (MGZ), bulk density, water content, and porosity. Laboratory procedures to determine the physical properties of the sediment samples followed the specifications for oceanographic survey GB/T 12763.8-2007 [34] and the standard for geotechnical testing method GB/T 50123-1999 [35], belonging to National Standard of the People's Republic of China. The wet bulk density is the weight of the mineral solids and porewater per unit volume and was measured using a cutting-ring method using a steel ring sampler (diameter 6 cm, height 2 cm) which was pushed into the sediment sample. The sampler with sediment core in it was weighed to determine the wet bulk density. The grain specific gravity was measured on dried samples with a pycnometer (volume 50 mL). Porosity is the ratio in percent of the volume of voids to the total volume of the sediment mass. Porosity was calculated for each sample using measurements of water content, wet bulk density and grain specific gravity. The calculation equation of porosity was,

$$e = \frac{\rho(1+w)}{\rho_s} - 1 \tag{1}$$

$$n = \frac{e}{1+e} \tag{2}$$

where e is the void ratio; ρ is wet bulk density; w is water content; ρ_s is grain specific gravity; n is porosity.

A sieving method was used to determine the composition, mean grain size, sand content, clay content, and sorting coefficient. The apertures of sieve include 2.0 mm, 1.0 mm, 0.5 mm, 0.25 mm, 0.1 mm, and 0.075 mm. The sediments were then classified using Shepard's ternary diagram [36] based on the obtained sand and clay contents. The mean grain size was determined by plotting the particle distribution curve and identifying the values corresponding to d16, d50, and d84.

4. Results

4.1. Sediment Types

Table 1 presents the particle composition and sediment types at all stations, with corresponding Shepard ternary diagram in Figure 3. Sections AB and CD exhibit distinct sediment distribution patterns. Four stations on section AB display varying sediment types, with finer sediments in shallow waters. Station A1 consists of silty sand with a high sand content of 63.8%, while stations A2 and A3 transition to higher silt content and lower clay content towards the outer shelf, categorized as silt and sandy silt, respectively. Station A4 is characterized by silt particles with a clay content of 33.4%, classified as clayey silt. In contrast, stations D1 to D5 on section CD have lower sand content, predominantly composed of silt and clay. Silt content ranges from 39.9% to 65.7%, and clay content is slightly lower, ranging from 32.9% to 54.2%. Stations D1, D4, and D5 have higher silt content, classified as clayey silt, while D2 and D3 have higher clay content, classified as silty clay. Despite the proximity of station A3 to D4 and D5 on section CD, its particle composition differs significantly. Conversely, station A4, located in deep water, shares similarities in sediment type and particle composition with the shallower water stations on section CD.

Table 1. Sediment type, particle component, and physical properties for each stations.

Station	Sediment Type	Sand Content (%)	Silt Content (%)	Clay Content (%)	Density (kg/m^3)	Porosity (%)	Mean Grain Size (ϕ)
A1	Silty sand	63.8	29.7	6.5	1876	48.6	3.994
A2	Silt	5.2	81.3	13.5	1574	66.4	6.018
A3	Sandy silt	18.0	71.2	10.8	1634	63.3	5.494
A4	Clayey silt	5.7	60.9	33.4	1406	76.7	7.231
D1	Clayey silt	1.7	56.0	42.3	1602	66.6	7.820
D2	Silty clay	2.8	48.0	49.2	1584	64.9	7.953
D3	Silty clay	5.9	39.9	54.2	1521	69.9	8.064
D4	Clayey silt	2.4	60.8	36.8	1599	64.9	7.108
D5	Clayey silt	1.4	65.7	32.9	1713	59.2	7.139

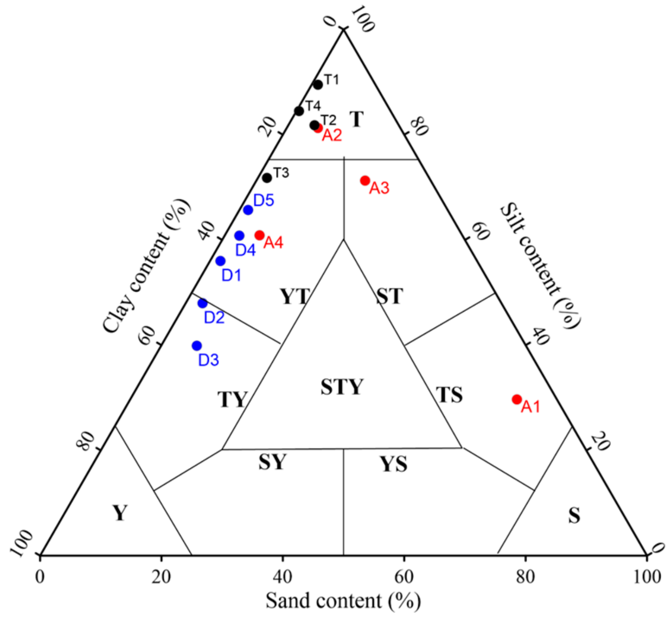

Figure 3. Shepard ternary diagram of sediment types in the experimental area. Red and blue dots represent particle composition at stations on sections AB and CD, respectively. The diagram also includes the percentage of sediment particle fractions at four stations in the West Pacific Ocean (black dots, data from Wang et al. [15]).

4.2. Acoustic Properties and Corresponding Physical Properties on Section AB

Tables 1 and 2 displays the physical and acoustic properties, respectively, and Figure 4 illustrates the variation of both acoustic and physical properties along the section AB. The acoustic and physical properties at each station exhibit significant variations in the down-slope direction, corresponding to changes in sediment type. Generally, as water depth increases from the shelf to the trough, acoustic properties (both in situ and in laboratory) and density decrease, while porosity and mean grain size increase. In situ acoustic speed ranges from 1446–1594 m/s, attenuation coefficient ranges from 0.89–7.63 dB/m, and SSR varies from 0.970–1.038. The laboratory acoustic speed ranges from 1473–1613 m/s, attenuation coefficient ranges from 14.91–47.28 dB/m, and SSR varies from 0.978–1.072. Physical properties show density ranging from 1406–1876 kg/m^3, porosity from 48.6–76.7%, and MGZ from 3.994–7.231 ϕ. As shown in the figure and tables, lab acoustic properties are consistently higher than in situ ones at all stations, with the most significant difference observed in attenuation, particularly at station A1. Station A1 stands out as having a SSR greater than 1, indicating higher sediment sound speed compared to seafloor seawater sound speed. For stations from the shelf edge to the trough, SSR values less than 1 imply that sediment sound speed is lower than seafloor seawater sound speed.

Table 2. Acoustic properties measured in situ and in laboratory for each stations. Acoustic properties include sound speed (V), sound speed ratio (SSR), attenuation coefficient (α), and attenuation factor (k); the subscript "insitu" and "lab" represent data acquisition using the in situ or laboratory measurement method, respectively.

Station	Depth (m)	V_{insitu} (m/s)	SSR_{insitu}	α_{insitu} (dB/m)	k_{insitu} (dB/m/kHz)	V_{lab} (m/s)	SSR_{lab}	α_{lab} (dB/m)	k_{lab} (dB/m/kHz)
A1	92	1594	1.038	7.63	0.254	1613	1.072	47.28	0.426
A2	143	1499	0.986	0.89	0.030	1486	0.988	18.84	0.170
A3	244	1499	0.994	1.48	0.049	1504	0.998	14.91	0.134
A4	1865	1446	0.970	3.96	0.132	1473	0.979	17.17	0.155
D1	385	—	—	—	—	1462	0.976	38.81	0.343
D2	379	—	—	—	—	1480	0.987	21.51	0.190
D3	356	—	—	—	—	1465	0.981	41.17	0.364
D4	298	—	—	—	—	1479	0.986	30.37	0.269
D5	376	—	—	—	—	1499	0.995	20.38	0.180

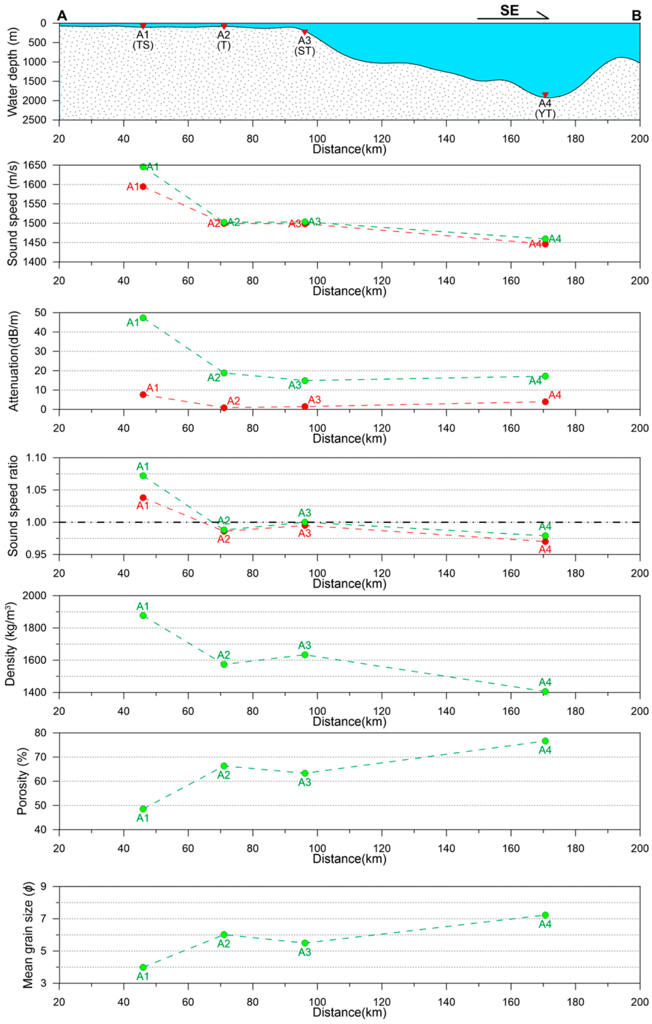

Figure 4. Variation of sediment acoustic and physical properties along section AB (NW-SE direction). Red dots represent acoustic properties measured using the in situ technique, and green dots represent acoustic and physical properties of sediment samples measured in the laboratory. The black dash-dotted line (SSR = 1) indicates that the sediment sound speed is equal to the overlying seawater sound speed.

4.3. Acoustic Properties and Corresponding Physical Properties on Section CD

Table 2 displays the acoustic properties of each station in section CD, while Table 1 presents the corresponding physical properties. Figure 5 illustrates the variations in acoustic and physical properties along the section, including station A3 at the intersection with section AB. The properties along this section exhibit distinct differences from those of section AB. From southwest to northeast, there is a consistent trend of increasing sound speed, SSR, and density, along with a gradual decrease in porosity and MGZ, but the variability of these parameters, except attenuation, is notably reduced compared to section AB. The laboratory sound speed ranged from 1462 to 1504 m/s, attenuation from 14.91 to 41.17 dB/m, and SSR from 0.976 to 0.998. In terms of physical properties, density ranged from 1521 to 1713 kg/m^3, porosity from 59.2% to 69.9%, and MGZ from 5.494 to 8.064 ϕ. Attenuation coefficient exhibited significant fluctuations along the section, ranging from 14.91 to 41.17 dB/m, with no distinct correlation observed with water depth or sediment type. Similar to station A3, SSR values of D1~D5 are all below 1, indicating that sediment sound speed near the shelf break is generally lower than seafloor seawater sound speed.

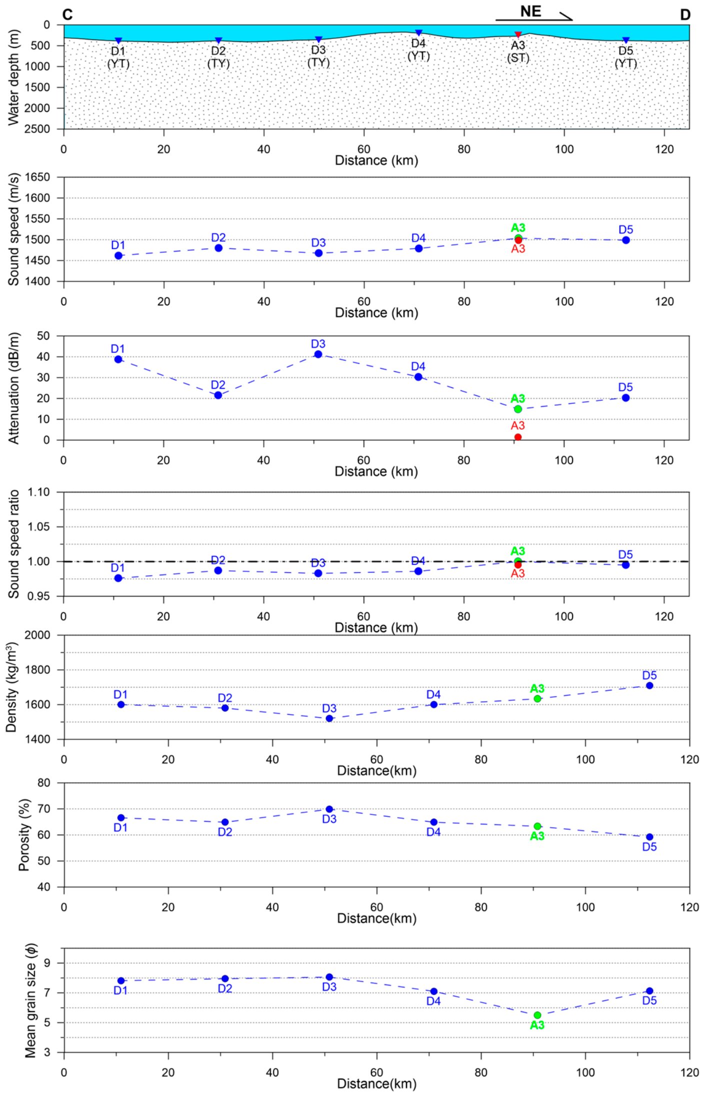

Figure 5. Variation of sediment acoustic and physical properties along section CD (SW-NE direction). Red dots represent acoustic properties measured using the in situ technique, and green and blue dots represent acoustic and physical properties of sediment samples measured in the laboratory. The black dash-dotted line (SSR = 1) indicates that the sediment sound speed is equal to the overlying seawater sound speed.

5. Discussion

5.1. Differences between In Situ and Laboratory Acoustic Properties Measurements

In the field work, sediment acoustics properties are typically obtained through in situ or laboratory techniques [3]. It is essential to compare the results from these two methods, considering the potential perturbation during sampling and measuring processes for the laboratory acoustic properties measurements. Richardson and Briggs [37] observed close agreement between laboratory and in situ measurements for gas-rich muddy sediments in Eckernförde Bay, Baltic Sea, and hard-packed sandy sediments in the northeastern Gulf of Mexico, despite differences in measurement frequencies (400 kHz in the laboratory and 58 kHz in situ). In contrast, Gorgas et al. [38] observed a little higher sound speed and greater attenuation measured in laboratory than in situ, in heterogeneous soft seabed sediments, Eel River shelf, and California.

In our experiment, in situ acoustic measurements were obtained at four stations in section AB, along with laboratory measurement using synchronously collected sediment samples. The comparison revealed varying degrees of differences between in situ and laboratory acoustic properties, with laboratory measurements generally higher for sound speed, sound speed ratio, and attenuation coefficient (Figure 4 and Table 2). This is consistent with the higher prediction of the laboratory acoustic–physical-property regressions than the in situ ones, particularly for sandy sediments [3]. Considering the frequency difference between in situ and laboratory measurement, the dispersion effect might be attributed to the higher laboratory acoustic properties [38], especially for sandy sediments, although the mechanism of acoustic attenuation dispersion remains debated [12,39–41]. Besides, sediment disturbance during sampling and transferring to the laboratory may also contribute to discrepancies between in situ and laboratory measurements. Li et al. [42] found shipboard measurements to align more closely with in situ measurements compared to laboratory results, particularly for fine-grained sediments, possibly due to perturbations and pore water loss or redistribution during the sample encapsulation, handling, and storage after their recovery.

In the case of deep-sea fine-grained sediments, the situation is different. Wang et al. [15] conducted in situ and laboratory sediment acoustic measurements from four stations (T1–T4 in Figure 3) in the western Pacific Ocean, with water depths exceeding 5000 m. The comparison also revealed discrepancies between the laboratory and in situ data, with higher sound speed ratios and attenuation coefficients in the laboratory results. These differences could not be fully explained by the frequencies dispersion based on poroelastic theoretical model, and the authors attributed them to sediment sample state changes caused by the deep-sea sample collection process. The water column pressure in deep sea might be another thinkable factor to explain this discrepancy. The weight of overlying water compacts seafloor sediments in their in situ state, thus increase their density and sound speed. Laboratory experiment had confirmed the sediment sound speed increase with increasing ambient pressure, but the sound speed ratio is almost invariable when the pressure change [31], meaning the water column pressure is negligible to affect the in situ and laboratory SSR discrepancy.

The findings in this experiment align well with existing knowledge. Station A1 has sand-dominated sediment, and shows higher laboratory acoustic properties, with the most significant deviation from its in situ ones. Stations A2 and A3 contain fine-grained sediment from shallower waters, with laboratory measurements closely matching in situ values. Station A4, despite also having fine-grained sediment, shows a larger discrepancy between laboratory and in situ measurements due to significant changes from deep-sea to laboratory conditions. These results highlight the need for caution when using laboratory acoustic measurements for both deep-sea and offshore coarse-grained sediments.

5.2. Relationship between Acoustic and Physical Properties

The variation trends of acoustic and physical properties along two sections (see Figures 4 and 5) demonstrates a strong correlation between them. Previous researches had established empirical equations linking these properties, enabling the prediction of acoustic properties from physical properties and vice versa [3,17,37,43,44]. While early equations were derived from laboratory data, recent studies have introduced empirical equations based on in situ measurements, which generally align in terms of trends, with some discrepancies existing [3,17].

To assess these equations for prediction of sound speed and attenuation based on physical properties, two classical and two recent empirical equations are chosen to compare with the measured data in this experiment. These equations are: (1) ISSAMS empirical equations, established by Richardson and Briggs [37] based on in situ measured data at 38 kHz or 58 kHz using in situ sediment acoustic measurements system (ISSAMS); (2) BISAMS empirical equations, established by Wang et al. [17] based on in situ measured data at 30 kHz using BISAMS; (3) R&B empirical equations, established by Richardson and Briggs [37] based on laboratory measured data at 400 kHz; (4) SCS empirical equations, established by Li et al. [44] based on laboratory measured data at 100 kHz. For ISSAMS, BISAMS, and R&B equations, the relationships of SSR and attenuation factors with density, porosity, and MGZ are included, while for SCS equations, only the relationships of SSR with density, porosity, and MGZ are discussed.

As presented in Figure 6a–f, both laboratory and in situ results in this experiment show good agreement with the SSR vs. density and SSR vs. porosity empirical equations. In section AB, in situ values fall between ISSAMS and BISAMS curves, while laboratory measurements fall between SCS and R&B curves. In section CD, laboratory values are slightly below SCS and R&B curves, while falling between the two in situ curves. In contrast, agreement between the measurements and empirical SSR vs. MGZ curves is low. Most in situ and laboratory values are below SSR vs. MGZ curves, indicating the limitation of acoustic prediction based on MGZ.

It is noteworthy that D1–D5 have MGZ values similar to A4, but closer density and porosity values to A2 and A3, which correlate better with SSR, also proving the poor prediction based on MGZ. In fact, the multiplicity of porosity vs. MGZ relationship had previously been noticed, as shown in Figure 7 in Buckingham [8], which he attributed to the difference of grain smoothness (Δ, rms roughness) in various sediment. Using different Δ to fit the measured porosity vs. MGZ relationship on the two sections, as shown in Figure 7, the good agreement of theoretical curves to measured data seems to confirm the assertions of Buckingham. As a sediment characteristic, MGZ only provides limited insight into the sedimentary environment, and other factors, such as sorting and psephicity, also influence sediment arrangement and therefore acoustic and physical characteristics. Consequently, predicting acoustic properties based solely on particle composition or MGZ is associated with higher uncertainty.

As far as the correlation between attenuation factor and physical properties, a general trend is that the attenuation factor decreases with porosity and MGZ and increases with density (Figure 6d–f). However, this correlation is weaker compared to that between SSR and physical properties. For in situ attenuation, the relationship between attenuation factor and density or porosity is close to the BISAMS curve for A2 to A3, and to the ISSAMS curve for A1 and A4 (Figure 6d,e). Stations A1–A3 show a close relationship between the attenuation factor and MGZ following the BISAMS curve, while station A4 roughly follows the ISSAMS curve (Figure 6f). For the relationship between laboratory attenuation and physical properties, all stations align more closely with the ISSAMS curves rather than the laboratory R&B curves. These results highlight the high uncertainty in predicting attenuation based on physical properties, as suggested by Jackson and Richardson [3].

To different degree the measured data depart from the previous equations, as shown in Figure 6a–f. Even among these equations differences also exist, not only between the in situ and laboratory ones, but also those based on same type of measurement technique. Jackson and Richardson [3] attribute it to difference between the acoustic measurement technology and the physical property measurement technology. Wang et al. [17] suggest the physical properties measurement in laboratory might contribute more to such discrepancy. During the measurement by different authors, the disturbances in the sample collection and measurement process varied to different degree, causing the measured physical properties depart various degree to the true value. As a result, the acoustical properties prediction based on empirical equations can only provide the preliminary estimation when the measured data are not available.

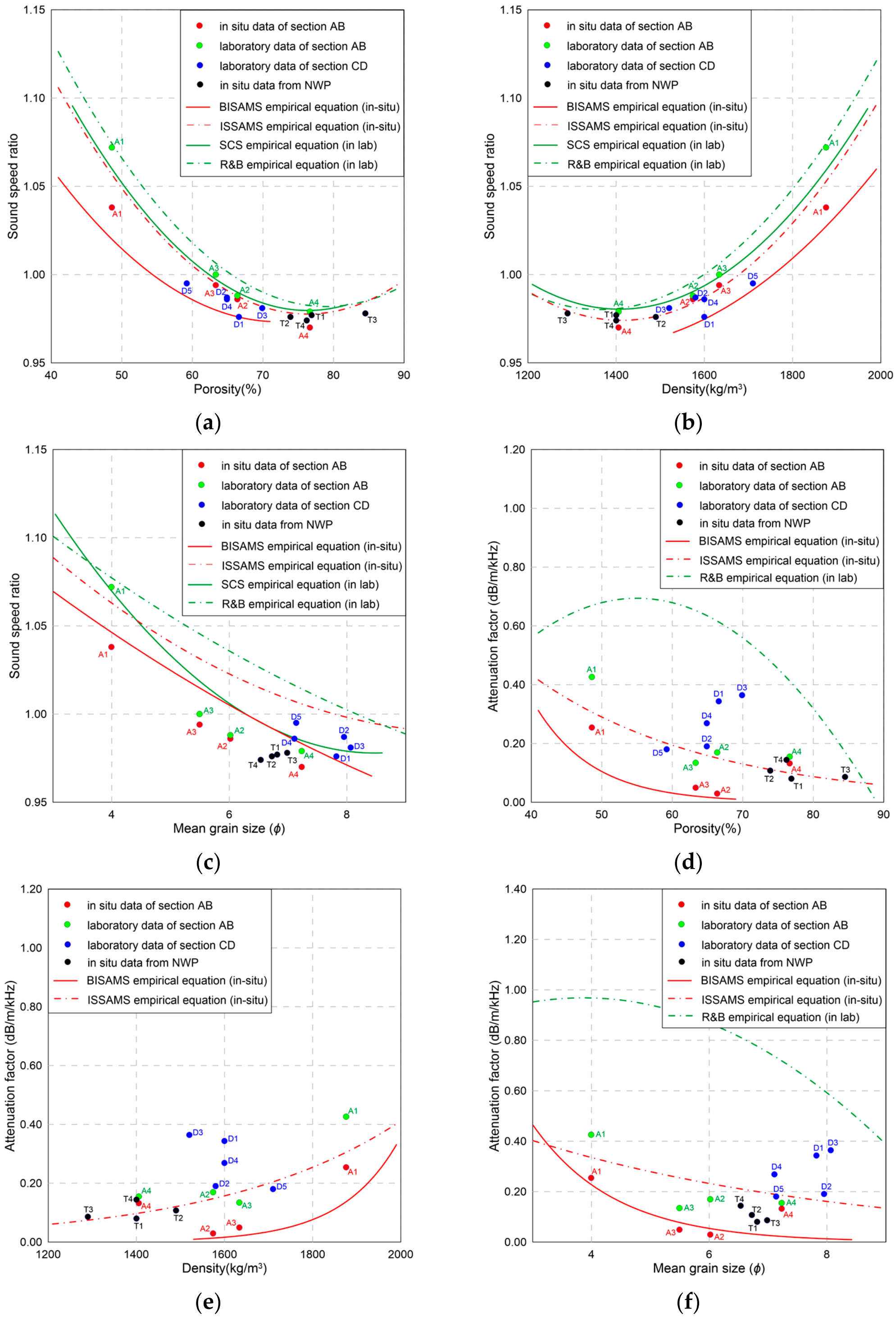

Figure 6. Relationship between measured acoustic properties and physical properties and their comparison with existing empirical relationship curves: (**a**) SSR vs. porosity, (**b**) SSR vs. density, (**c**) SSR vs. MGZ, (**d**) attenuation factor vs. porosity, (**e**) attenuation factor vs. density, and (**f**) attenuation factor vs. MGZ.

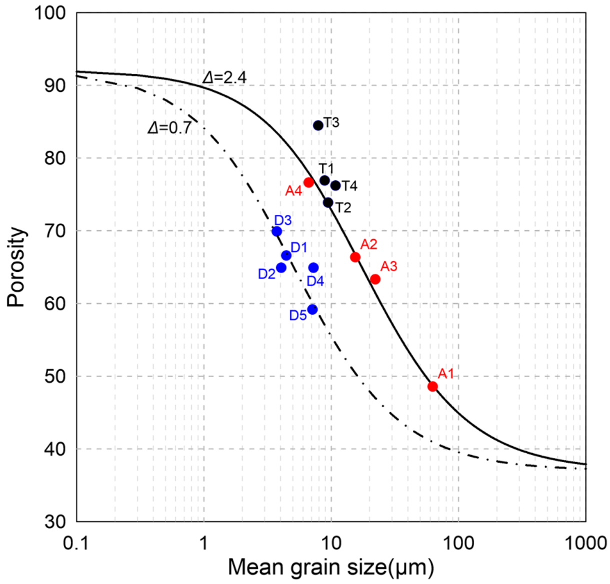

Figure 7. Relationship between measured porosity and MGZ (dots in different colors), with comparison to theoretical curves (solid and dotted lines) calculated from Equation (17) of Buckingham [45]. Note the difference of Δ (rms roughness) taken for the two curves.

5.3. Sedimentary Environment Controls on Sediment Acoustic Properties

Sediment acoustic properties are inherent characteristics of sediments, closely linked to their composition and structure, which are influenced by the environmental conditions during their formation [3,4,6]. In the study area, sediment acoustic properties and physical properties exhibit significant down-slope changes and gradual along-slope changes. These variations are associated with regional sediment distribution patterns and the sedimentary environment.

The study area is situated in the continental terrace in the north-western part of the South China Sea. Continental terraces serve as crucial pathways for terrigenous materials between continents and oceans, playing a significant role in the Earth's source-sink system [46]. Rivers transport a substantial amount of terrigenous materials to the shelf and slope, where they are deposited, or further carried to the open ocean by ocean dynamics [47]. In the South China Sea, coastal currents and deep currents, associated with the East Asian monsoon, the Kuroshio current, and Western Pacific deep waters passing through the Luzon Strait are prominent factors to mold the sediment distribution pattern [48–52]. Studies had identified multiple sources of sediment in different regions of this area. Sediments on the shelf and slope primarily originate from the Red River and small rivers on Hainan Island [22]. In the trough, sediment transport is influenced by gravity currents and materials from Taiwan Island through bottom currents in the northern South China Sea [23]. On the shelf, sediments exhibit a zonal distribution parallel to the shoreline, with coarser sediments closer to land and finer sediments outside [24], resulting in the gradual reduction of the acoustic properties away from the Hainan Island. The distribution pattern along the terraces remains stable, with fine-grained sediments from the Red River transported over long distances and decreasing in clay content towards the northeast due to the blockage by Hainan Island [26]. Conversely, short-distance transport from Hainan Island increases, leading to an increase in relatively coarse-grained material and a decrease in clay content towards the northeast [22], potentially contributing to the increase in acoustic properties in that direction.

The deep-sea deposits at station A4 exhibit unique characteristics compared to other stations. While their particle composition is similar to stations D1–D5 on the outer shelf, the physical and acoustic properties of A4 differ significantly (Tables 1 and 2). In contrast, stations in the deep western Pacific Ocean show similar acoustic and physical properties to

A4 (Figure 3), despite differences in particle composition. This highlights the influence of deep sea environment on the sediment acoustic properties.

6. Conclusions

Acoustic and physical properties of the seabed in the northwestern South China Sea were studied through in situ and laboratory measurements on the shelf and slope along two sections: down-slope and along-slope. The analysis of the results revealed the following conclusions:

(1) Acoustic properties of seafloor sediments exhibit systematic changes with increasing offshore distance and water depth from the shelf to the slope, showing significant decreases in sound speed and attenuation in the down-slope direction. In the along-slope direction, especially near the shelf break, acoustic speed and attenuation are relatively consistent or change minimally compared to the down-slope direction.

(2) Discrepancies exist between acoustic properties obtained from in situ and laboratory measurements, particularly for deep-sea and offshore coarse-grained sediments. Caution should be exercised when using laboratory measurements for these sediment types, with preference given to in situ measurements.

(3) Comparison of measured acoustic properties with predictions from empirical equations for acoustic-physical properties indicates that predicted sound speed using density and porosity aligns more closely with measured results, while predicted sound attenuation shows inconsistencies. Predictions based on mean grain size result in deviations in both sound speed and attenuation, highlighting limitations of the empirical prediction method.

(4) Changes in acoustic properties of seafloor sediments on the shelf and slope are influenced by material sources, hydrodynamic conditions, and water depth. Regional variations in acoustic properties are more prominent on the shelf due to source influence and shallow-water hydrodynamics, while properties on the slope and in deep water are primarily controlled by water depth.

Author Contributions: Conceptualization, G.L.; methodology, J.W. and X.M.; validation, G.L., G.K., and C.L.; formal analysis, G.L. and J.W.; investigation, G.L. and Q.H.; data curation, G.K.; writing—original draft preparation, G.L. and J.W.; writing—review and editing, G.L. and G.K.; visualization, Q.H. and C.L.; supervision, C.L.; project administration, G.L.; funding acquisition, G.L. All authors have read and agreed to the published version of the manuscript.

Funding: This research was funded by National Natural Science Foundation of China under contract No. 42076082, Laoshan Laboratory under contract No. LSKJ202204802, Shandong Provincial Natural Science Foundation under contract No. DKXZZ202206.

Institutional Review Board Statement: Not applicable.

Informed Consent Statement: Not applicable.

Data Availability Statement: Data are contained within the article.

Acknowledgments: The authors thank the crew of R/V Shiyan 1 for their assistance in field data acquisition and samples collection.

Conflicts of Interest: The authors declare no conflict of interest.

References

1. Katsnelson, B.; Petnikov, V.; Lynch, J. *Fundamentals of Shallow Water Acoustics*; Springer: New York, NY, USA, 2012; pp. 55–62.
2. Frisk, G.V. *Ocean and Seabed Acoustics: A Theory of Wave Propagation*; P T R Prentice-Hall: Upper Saddle River, NJ, USA, 1994; pp. 1–16.
3. Jackson, D.R.; Richardson, M.D. *High-Frequency Seafloor Acoustics*; Springer: New York, NY, USA, 2007; pp. 134–170.
4. Kim, S.R.; Lee, G.S.; Kim, D.C.; Bae, S.H.; Kim, S.P. Physical properties and geoacoustic provinces of surficial sediments in the southwestern part of the Ulleung Basin in the East Sea. *Quat. Int.* **2017**, *459*, 35–44. [CrossRef]
5. Hamilton, E.L. Sound velocity and related properties of marine sediments, North Pacific. *J. Geophys. Res.* **1970**, *75*, 4423–4446. [CrossRef]

6. Hamilton, E.L. Geoacoustic modelling of the seafloor. *J. Acoust. Soc. Am.* **1980**, *68*, 1313–1340. [CrossRef]
7. Williams, K.L.; Jackson, D.R.; Thorsos, E.I.; Tang, D.; Schock, S.G. Comparison of sound speed and attenuation measured in a sandy sediment to predictions based on the Biot theory of porous media. *IEEE J. Ocean. Eng.* **2002**, *27*, 413–428. [CrossRef]
8. Buckingham, M.J. Compressional and shear wave properties of marine sediments: Comparisons between theory and data. *J. Acoust. Soc. Am.* **2005**, *117*, 137–152. [CrossRef] [PubMed]
9. Zhou, J.; Zhang, X.; Knobles, D.P. Low-frequency geoacoustic model for the effective properties of sandy seabottoms. *J. Acoust. Soc. Am.* **2009**, *125*, 2847–2866. [CrossRef]
10. Hines, P.C.; Osler, J.C.; Scrutton, J.G.E.; Halloran, L.J.S. Time-of-flight measurements of acoustic wave speed in a sandy sediment at 0.6–20 kHz. *IEEE J. Ocean. Eng.* **2010**, *35*, 502–515. [CrossRef]
11. Yang, J.; Tang, D. Direct measurements of sediment sound speed and attenuation in the frequency band of 2–8 kHz at the Target and Reverberation Experiment site. *IEEE J. Ocean. Eng.* **2017**, *42*, 1102–1109. [CrossRef]
12. Chotiros, N.P. *Acoustics of the Seabed as a Poroelastic Medium*; Springer: New York, NY, USA, 2017; pp. 7–24. [CrossRef]
13. Wang, J.; Guo, C.; Hou, Z.; Fu, Y.; Yan, J. Distributions and vertical variation patterns of sound speed of surface sediments in South China Sea. *J. Asian Earth Sci.* **2014**, *89*, 46–53. [CrossRef]
14. Tian, Y.; Chen, Z.; Hou, Z.; Luo, Y.; Xu, A.; Yan, W. Geoacoustic provinces of the northern South China Sea based on sound speed as predicted from sediment grain size. *Mar. Geophy. Res.* **2019**, *40*, 571–579. [CrossRef]
15. Wang, J.; Li, G.; Kan, G.; Liu, B.; Meng, X. Experimental study on in situ measurement of acoustic characteristics of deep seabed sediments. *Chin. J. Geophy.* **2020**, *63*, 4463–4472, (In Chinese with English abstract).
16. Liu, B.; Han, T.; Kan, G.; Li, G. Correlations between the in situ acoustic properties and geotechnical parameters of sediments in the Yellow Sea, China. *J. Asian Earth Sci.* **2013**, *77*, 83–90. [CrossRef]
17. Wang, J.; Kan, G.; Li, G.; Meng, X.; Zhang, L.; Chen, M.; Liu, C.; Liu, B. Physical properties and in situ geoacoustic properties of seafloor surface sediments in the East China Sea. *Front. Mar. Sci.* **2023**, *10*, 1195651. [CrossRef]
18. Li, G.; Wang, J.; Liu, B.; Meng, X.; Kan, G.; Han, G.; Hua, Q.; Pei, Y.; Sun, L. In situ acoustic properties of fine-grained sediments on the northern continental slope of the South China Sea. *Ocean Eng.* **2020**, *218*, 108244. [CrossRef]
19. Li, K.Z.; Yin, J.Q.; Huang, L.M.; Lian, S.M.; Zhang, J.L.; Liu, C.G. Monsoon forced distribution and assemblages of appendicularians in the northwestern coastal waters of South China Sea. *Estuar. Coast. Shelf Sci.* **2010**, *89*, 145–153. [CrossRef]
20. Zheng, H.B.; Yan, P. Deep-water bottom current research in the Northern South China Sea. *Mar. Georesour. Geotechnol.* **2012**, *30*, 122–129.
21. Liu, Z.; Tuo, S.; Colin, C.; Liu, J.T.; Huang, C.-Y.; Selvaraj, K.; Chen, C.-T.A.; Zhao, Y.; Siringan, F.P.; Boulay, S.; et al. Detrital fine-grained sediment contribution from Taiwan to the northern South China Sea and its relation to regional ocean circulation. *Mar. Geol.* **2008**, *255*, 149–155. [CrossRef]
22. Liu, J.; Clift, P.D.; Yan, W.; Chen, Z.; Chen, H.; Xiang, R.; Wang, D. Modern transport and deposition of settling particles in the northern South China Sea: Sediment trap evidence adjacent to Xisha Trough. *Deep Sea Res. Part I* **2014**, *93*, 145–155. [CrossRef]
23. Xu, F.J.; Hu, B.Q.; Dou, Y.G.; Liu, X.T.; Wan, S.M.; Xu, Z.K.; Tian, X.; Liu, Z.Q.; Yin, X.B.; Li, A.C. Sediment provenance and paleoenvironmental changes in the northwestern shelf mud area of the South China Sea since the mid-Holocene. *Cont. Shelf Res.* **2017**, *144*, 21–30. [CrossRef]
24. Shi, X.F. *China Marine Offshore-Seabed Sediment*; China Ocean Press: Beijing, China, 2012; pp. 1–561. (In Chinese)
25. Liu, Z.; Colin, C.; Li, X.; Zhao, Y.; Tuo, S.; Chen, Z.; Siringan, F.P.; Liu, J.T.; Huang, C.-Y.; You, C.-F.; et al. Clay mineral distribution in surface sediments of the northeastern South China Sea and surrounding fluvial drainage basins: Source and transport. *Mar. Geol.* **2010**, *277*, 48–60. [CrossRef]
26. Zhao, R.; Chen, S.; Olariu, C.; Steel, R.; Zhang, J.; Wang, H. A model for oblique accretion on the South China Sea margin; Red River (Song Hong) sediment transport into Qiongdongnan Basin since Upper Miocene. *Mar. Geol.* **2019**, *416*, 106001. [CrossRef]
27. GEBCO Compilation Group. GEBCO 2023 Grid. Available online: https://doi.org/10.5285/f98b053b-0cbc-6c23-e053-6c86abc0af7b (accessed on 1 August 2023).
28. Wang, J.; Li, G.; Liu, B.; Kan, G.; Sun, Z.; Meng, X. Experimental study of the ballast in situ sediment acoustic measurement system in South China sea. *Mar. Georesour. Geotechnol.* **2018**, *36*, 515–521. [CrossRef]
29. Hamilton, E.L. Prediction of in situ acoustic and elastic properties of seafloor sediments. *Geophysics* **1971**, *36*, 266–284. [CrossRef]
30. Zou, D.P.; Williams, K.L.; Thorsos, E.I. Infuence of temperature on acoustic sound speed and attenuation of seafloor sand sediment. *IEEE J. Oceanic Eng.* **2015**, *40*, 969–980. [CrossRef]
31. Kan, G.; Zou, D.; Liu, B.; Wang, J.; Meng, X.; Li, G.; Pei, Y. Correction for effects of temperature and pressure on sound speed in shallow seafloor sediments. *Mar. Georesources Geotechnol.* **2019**, *37*, 1217–1226. [CrossRef]
32. Wang, J.; Li, G.; Kan, G.; Hou, Z.; Meng, X.; Liu, B.; Liu, C.; Sun, L. High frequency dependence of sound speed and attenuation in coral sand sediments. *Ocean Eng.* **2021**, *234*, 109215. [CrossRef]
33. Hou, Z.; Chen, Z.; Wang, J.; Zheng, X.; Yan, W.; Tian, Y.; Luo, Y. Acoustic characteristics of seafloor sediments in the abyssal areas of the South China Sea. *Ocean Eng.* **2018**, *156*, 93–100. [CrossRef]
34. *GB/T 12763.8-2007 (National Standards of People's Republic of China)*; Specifications for Oceanographic Survey—Part 8: Marine Geology and Geophysics Survey. General Administration of Quality Supervision, Inspection and Quarantine of the People's Republic of China and National Standardization Management Committee of China: Beijing, China, 13 August 2007.

35. *GB/T 50123-1999 (National Standards of People's Republic of China)*; Standard for Soil Test Method. General Administration of Quality Supervision and Inspection and Quarantine of the People's Republic of China: Beijing, China, 10 June 1999.
36. Shepard, F.P. Nomenclature based on sand-silt-clay ratios. *J. Sediment. Res.* **1954**, *24*, 151–158.
37. Richardson, M.D.; Briggs, K.B. In situ and laboratory geoacoustic measurements in soft mud and hard-packed sand sediments: Implications for high-frequency acoustic propagation and scattering. *Geo-Mar. Lett.* **1996**, *16*, 196–203. [CrossRef]
38. Gorgas, T.J.; Wilkens, R.H.; Fu, S.S.; Frazer, L.N.; Richardson, M.D.; Briggs, K.B.; Lee, H. In situ acoustic and laboratory ultrasonic sound speed and attenuation measured in heterogeneous soft seabed sediments: Eel river shelf, California. *Mar. Geol.* **2002**, *182*, 103–119. [CrossRef]
39. Buckingham, M.J. On pore-fluid viscosity and the wave properties of saturated granular materials including marine sediments. *J. Acoust. Soc. Am.* **2007**, *122*, 1486–1501. [CrossRef]
40. Buckingham, M.J. Wave speed and attenuation profiles in a stratified marine sediment: Geo-acoustic modeling of seabed layering using the viscous grain shearing theory. *J. Acoust. Soc. Am.* **2020**, *148*, 962–974. [CrossRef] [PubMed]
41. Chotiros, N.P.; Isakson, M.J. Comments on "Pore fluid viscosity and the wave properties of saturated granular materials including marine sediments" [J. Acoust. Soc. Am. 122, 1486–1501 2007]". *J. Acoust. Soc. Am.* **2010**, *127*, 2095–2098. [CrossRef] [PubMed]
42. Li, G.; Kan, G.; Meng, X. Effect of the condition changes on the laboratory acoustic velocity measurements of seafloor sediments. *Adv. Mar. Sci.* **2013**, *31*, 360–366, (In Chinese with English abstract).
43. Hamilton, E.L.; Bachman, R.T. Sound velocity and related properties of marine sediments. *J. Acoust. Soc. Am.* **1982**, *72*, 1891–1904. [CrossRef]
44. Li, G.B.; Hou, Z.Y.; Wang, J.Q.; Kan, G.M.; Liu, B.H. Empirical equations of p-wave velocity in the shallow and semi-deep sea sediments from the South China Sea. *J. Ocean Univ. China* **2021**, *20*, 532–538. [CrossRef]
45. Buckingham, M.J. Theory of acoustic attenuation, dispersion, and pulse propagation in unconsolidated granular materials including marine sediments. *J. Acoust. Soc. Am.* **1997**, *102*, 2579–2596. [CrossRef]
46. Liu, Z.F.; Zhao, Y.L.; Colin, C.; Stattegger, K.; Wiesner, M.G.; Huh, C.A. Source-to-sink transport processes of fluvial sediments in the South China Sea. *Earth Sci. Rev.* **2016**, *153*, 238–273. [CrossRef]
47. Liu, J.P.; Xue, Z.; Ross, K.; Wang, H.J.; Yang, Z.S.; Li, A.C.; Gao, S. Fate of sediments delivered to the sea by Asian large rivers: Long-distance transport and formation of remote along shore clinothems. *SEPM Sediment. Rec.* **2009**, *7*, 4–9. [CrossRef]
48. Fang, G.H.; Fang, W.D.; Fang, Y.; Wang, K. A survey of studies on the South China Sea upper ocean circulation. *Acta Oceanogr. Taiwan* **1998**, *37*, 1–16.
49. Caruso, M.J.; Gawarkiewicz, G.G.; Beardsley, R.C. Interannual variability of the Kuroshio intrusion in the South China Sea. *J. Oceanogr.* **2006**, *62*, 559–575. [CrossRef]
50. Qu, T.D.; Girton, J.B.; Whitehead, J.A. Deepwater overflow through Luzon Strait. *J. Geophys. Res.* **2006**, *111*, C01002. [CrossRef]
51. Zhao, W.; Zhou, C.; Tian, J.W.; Yang, Q.X.; Wang, B.; Xie, L.L.; Qu, T.D. Deep water circulation in the Luzon Strait. *J. Geophys. Res. Oceans* **2014**, *119*, 790–804. [CrossRef]
52. Liu, J.G.; Clift, P.D.; Yan, W.; Chen, Z.; Chen, H.; Xiang, R. Temporal and spatial patterns of sediment deposition in the northern South China Sea over the last 50,000 years. *Palaeogeogr. Palaeoclimatol. Palaeoecol.* **2017**, *465*, 212–224. [CrossRef]